THE ASTROPHYSICAL JOURNAL, 370:615–629, 1991 April 1

HELIUM STAR CATACLYSMICS[1]

ICKO IBEN, JR.
Astronomy Department, Pennsylvania State University, 525 Davey Laboratory, University Park, PA 16802
AND
ALEXANDER V. TUTUKOV
Astronomical Council of the USSR, Academy of Sciences, 48 Pyatnitskaya Street, Moscow 109012, USSR
Received 1990 May 14; accepted 1990 September 13

ABSTRACT

Scenarios for close binary star evolution suggest that there is a finite probability ($\nu \sim 0.01$ yr^{-1}) for the formation of systems in which a carbon-oxygen white dwarf is accreting helium from a nondegenerate companion that is burning helium in its core. If it is gravitational wave radiation alone which drives mass transfer, the mass-transfer rate in such systems is approximately $3 \times 10^{-8}\ M_\odot$ yr^{-1}, remarkably insensitive to the mass ratio of the components. In typical systems, with orbital periods in the range 13–45 minutes, the donor with mass 0.3–1 $M_\odot$ has a luminosity between 4 $L_\odot$ and 250 $L_\odot$ and a surface temperature between 30,000 K and 50,000 K; the disk has a luminosity of the order of 100 $L_\odot$ and a temperature of about 40,000–70,000 K. There are several systems within 100 pc of the Sun, about 300 within 1 kpc of the Sun in the Galactic disk, and 10^5 in the entire Galaxy. The mass-transfer rate is approximately 300 times larger than that anticipated for classical hydrogen-transferring cataclysmic variables with orbital periods less than 2 hr and the lifetime is some 200 times smaller than that of short-period classical cataclysmics. After the transfer of $\sim 0.15\ M_\odot$ of helium onto a dwarf of initial mass 0.6–1 $M_\odot$, a thermonuclear runaway occurs in the accreted layer. If the mass of the accretor is $\sim 0.6\ M_\odot$, the resulting outburst may qualitatively resemble a normal nova, except that no hydrogen lines appear in the spectrum, the total nuclear energy released is much larger than in the case of a nova, and the mass of the ejectum is comparable with that of a planetary nebula. In fact, the system may very well appear as a short-lived helium planetary nebula, once ejection has been completed and the remnant star has contracted sufficiently to achieve surface temperatures larger than 50,000 K. If it remains visible for ~ 100 yr, there may be one such super nova at any time in the Galaxy at a luminosity of the order of $10^4\ L_\odot$. If the mass of the accretor is 1 $M_\odot$ or larger, an explosion of weak (dwarf) supernova magnitude will occur. Perhaps two in 10 supernovae may be of this variety, and supernova 1885A in Andromeda is a possible example. The critical accretor mass which separates the two types of behavior is of the order of $0.8\ M_\odot$.

Subject headings: stars: binaries — stars: dwarf novae — stars: evolution — stars: interiors — stars: novae — stars: supernovae — stars: white dwarfs

1. HOW ARE THEY MADE?

There are several evolutionary scenarios for producing helium star cataclysmics (see, e.g., Tornambè & Matteucci 1986; Iben & Tutukov 1987; Tutukov & Fedorova 1989). As an example, consider systems in which both components are of comparable mass in the mass range 2.5–8 $M_\odot$ at a separation A_0 such that the primary fills its Roche lobe after it has exhausted central helium to become an asymptotic giant branch (AGB) star with an electron-degenerate carbon-oxygen (CO) core. The orbital separation is larger than along the line labeled "helium burning in the primary" in Figure 1. Since the primary has a deep convective envelope, a common envelope phase is inevitable. Mass transfer will continue until the primary has lost most of its hydrogen-rich envelope. The mass of the remnant, which rapidly evolves into a CO white dwarf, is almost independent of whether Roche-lobe filling occurs during the early AGB phase or during the thermally pulsing AGB phase (Iben 1986) and remnant mass M_{1R} and initial primary mass M_1 are related approximately by

$$M_{1R} \sim 0.275\ M_1^{2/3}\ , \qquad (1)$$

where masses are in solar units. Unless otherwise noted, masses and distances will hereinafter be understood to be in solar units.

Frictional interaction between the orbiting stellar pair and the common envelope produces energy which forces the common envelope to expand until its radius exceeds the maximum radius of a star of comparable mass in hydrostatic equilibrium ($R_{\max} \sim 1000\ R_\odot$). The time scale on which the envelope then disrupts may be estimated (Paczyński 1976; Meyer & Meyer-Hofmeister 1979; Iben & Tutukov 1984a) to be $\tau_{\rm loss} \sim 10^{-3}\ R_{\max}^2\ M_1^{-1/2}$ yr; for $R_{\max} \sim 10^3$, $\tau_{\rm loss} \sim 10^3/M_1$ yr. This time is very short and the mass of the secondary cannot change significantly during the common envelope phase. The final semimajor axis after the common envelope stage may be estimated to be (Iben & Tutukov 1984a)

$$A_f = (\alpha/2)(M_{1R}/M_1)(M_2/M_1)A_0\ , \qquad (2)$$

where α is a parameter of the order of unity (say, 0.5–1.0). Two-dimensional hydrodynamic calculations (Livio & Socker 1988; Taam & Bodenheimer 1989) and an examination of the properties of close central stars of planetary nebulae (Iben & Tutukov 1989a) support this estimate. Most of the initial orbital angular momentum is lost from the system in the mass-loss process, and the orbital size decreases by a large factor.

[1] Supported in part by the National Science Foundation grant AST 88-07773 and in part by endowment funds for the Eberly Family Chair in Astronomy and Astrophysics at the Pennsylvania State University.

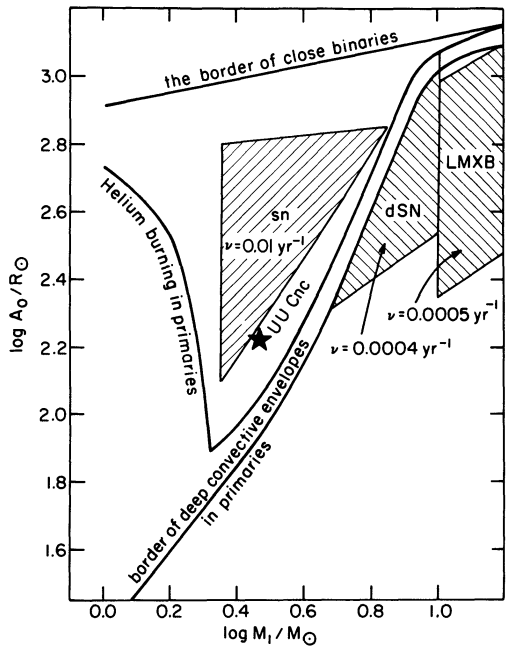

FIG. 1.—The semimajor axis (A_0) – primary mass (M_1) diagram. The radius of the primary is transformed into the semimajor axis on the assumption that the initial masses of the components are the same. The core helium-burning ignition line is taken from Maeder & Meynet (1989). The other borders are presented in the text.

The system now consists of a CO degenerate dwarf and a main sequence star that will fill its Roche lobe before helium burning begins (see Fig. 1).

Because of the large mass ratio of the components, a common envelope is formed once again when the second star overfills its Roche lobe, and frictional interaction between the double stellar cores—the CO degenerate dwarf remnant of the primary and the non-degenerate helium core of the secondary—will once again lead to evaporation of the common envelope and to orbital shrinkage, the extent of which may be estimated from the expression

$$A_{\rm ff} = (\alpha/2)^2(M_{1R}/M_1)^2(M_{2R}/M_2)A_0 , \quad (3)$$

where M_{2R} is the mass of the helium-star remnant of the secondary. In first approximation (Iben & Tutukov 1985),

$$M_{2R} = 0.1M_2^{5/4} . \quad (4)$$

Inserting this expression and equation (1) into expression (3) gives

$$A_{\rm ff} = 0.0019M_2^{1/4}M_1^{-2/3}\alpha^2 A_0 . \quad (3')$$

In most instances, the helium star remnant will not fill its Roche lobe when the common envelope phase is completed. On the other hand, the orbital separation continues to decrease due to the radiation of gravitational waves. The time required for the separation of two orbiting point objects of mass $M_{\rm He}$ and $M_{\rm CO}$, respectively, to decrease from an initial separation $A_{\rm ff}$ to zero in response to the emission of gravitational wave radiation is

$$\tau_{\rm GW}\ ({\rm yr}) = 10^{8.2}A_{\rm ff}^4/(M_{\rm He}M_{\rm CO}[M_{\rm He} + M_{\rm CO}]) . \quad (5)$$

The helium-burning lifetime of the helium star is (Iben & Tutukov 1985; Iben 1990)

$$\tau_{\rm He}\ ({\rm yr}) \sim 10^{7.1}M_{\rm He}^{-3.2} , \quad (6)$$

and, if we require that $\tau_{\rm He} > \tau_{\rm GW}$, we have that

$$A_0 < 10^{2.8}\alpha^{-2}q^{-1}M_2^{1/16}(1 + 0.36q^{2/3}M_2^{7/12})^{1/4} , \quad (7)$$

where $q = M_2/M_1$. To a good approximation, this condition is equivalent to

$$A_0 < 10^{2.8}\alpha^{-2}q^{-1} . \quad (7')$$

This translates also into $A_{\rm ff} < 0.985M_1^{-1/3}M_2^{-1/4}$.

A lower limit on A_0 follows from the requirement that the helium star does not fill its Roche lobe immediately after the dissipation of the common envelope. The relationship between mass and radius for a helium star of homogeneous composition is approximately (Iben 1990)

$$R_{\rm He} = 0.20M_{\rm He}^{0.88} , \quad (8)$$

and using a simple approximation to the relationship between orbital separation and Roche-lobe radius (Iben & Tutukov 1984a),

$$R_L \sim 0.52(M_{\rm He}/[M_{\rm He} + M_{\rm CO}])^{0.44}A_{\rm ff} , \quad (9)$$

the lower limit is found to be

$$A_0 > 42\alpha^{-2}M_1^{0.95}M_2^{0.3}(1 + 0.36q^{2/3}M_2^{7/12})^{0.44} . \quad (10)$$

Limits defined by equations (7) and (10) are drawn in Figure 1 for $\alpha = 1$, and the permitted values of A_0 and M_1 lie in the hatched region labeled "sn" (for super nova). The permitted region lies above the border for components with deep convective envelopes, thus justifying our initial assumption of non-conservative evolution after the primary fills its Roche lobe. We are aware of at least one binary system which has a semimajor axis lying within the permitted region and in which the primary is just at the beginning of the fast mass-exchange phase. This system is UU Cnc (Barone et al. 1988), and the mass-exchange rate in this system is now about $4 \times 10^{-3}\ M_\odot\ {\rm yr}^{-1}$.

The frequency of formation of systems consisting of a helium nondegenerate star which can transfer mass to a companion CO degenerate dwarf can be estimated (Iben & Tutukov 1984a) from the expression

$$d^3\nu\ ({\rm yr}^{-1}) = 0.2\,d\ \log\ A_0(dM_1/M_1^{2.5})dq . \quad (11)$$

From Figure 1 we obtain a frequency of formation $\nu_A \sim 0.01\ {\rm yr}^{-1}$, and estimate that the mass of the CO dwarf is less than $0.8\ M_\odot$ in approximately 80% of the systems formed. The frequency estimate could easily be wrong by a factor of 3 or more.

Observational counterparts of the predicted systems presumably are hidden among subdwarf O and B stars. Many of these may be single stars which are the consequences of mergers of helium degenerate dwarfs; such single sdO and sdB stars are estimated to be formed at a rate of about $0.1\ {\rm yr}^{-1}$ (Iben & Tutukov 1990), again with an uncertainty which could be as large as a factor of 3. Our estimates suggest that as many as 10% of all sdOB stars could be in a binary (with a CO companion) with periods in the range 13 minutes–6 hr and semiamplitudes of radial velocity variations in the range 100–500 km s^{-1} (Tutukov & Yungelson 1990). The observational search for such objects is only in the beginning stages. Studying a sample of 39 sdO and sdB stars, Saffer & Liebert (1989) have found three stars with radial velocity larger than 100 km s^{-1}, and the radial velocity of one of these is known to vary. Orbital periods are not yet known.

Several additional, less frequently occurring scenarios are discussed by Tutukov & Yungelson (1990). One scenario begins with systems with small initial q in which the primary, of mass in the range 5–10 $M_\odot$, fills its Roche lobe before it ignites helium. As the properties of ordinary cataclysmic variables (a massive CO degenerate dwarf in a tight orbit with a low mass main sequence star) demonstrate, the low initial mass ratio ensures that the first phase of mass transfer leads to the establishment of a common envelope and extensive orbital shrinkage, whether or not the primary has developed a deep convective envelope. An application of the principles used to set limits on A_0 when the primary fills its Roche lobe after having exhausted helium at the center (case C event) gives in the present instance (case B event)

$$26\alpha^{-2}M_1^{3/5}M_2^{0.85}M_{\rm IR}^{-1} < A_0 < 750\alpha^{-2}M_1^{3/5}M_2^{-0.94}M_{\rm IR}^{-0.5}\,, \tag{12}$$

where M_R is the final mass of the primary remnant, which can be a white dwarf or a neutron star. Assuming that $q < \frac{1}{2}$, $M_{\rm IR} = 0.8$ for $4.5 < M_1 < 10$, $M_R \sim 1.4$ for $M_1 > 10$, and $M_2 > 2.5$ results in the hatched permitted region in Figure 1 labeled dSN (for dwarf supernova). The lower border of this region is determined by excluding all situations in which the helium core of the donor is swallowed by the accretor. For details of this estimate see Tutukov & Yungelson (1990).

Again using expression (11), we estimate the realization frequency for this channel to be $\nu_B \sim 0.0007$ yr^{-1}, with an uncertainty of a factor of 3. The masses of the accreting CO dwarf components are all larger than about 0.8 $M_\odot$.

We conclude this introduction by commenting on a scenario which leads to the formation of systems consisting of a neutron star fed by a helium-star secondary. Such systems bear the same relationship to the bulge low-mass X-ray binaries (LMXBs) as the helium star CVs bear to classical CVs. The permitted region for initial primary mass and orbital separation is the hatched region in Figure 1 labeled LMXB (Tutukov 1988). The primary evolves into a neutron star and, after a final common envelope stage, the secondary, of initial mass in the 2.3–5 $M_\odot$ range, evolves into a nondegenerate helium star of mass in the 0.3–0.8 $M_\odot$ range. The components are driven together by gravitational wave radiation and the system evolves into a very short period LMXB fueled by accretion of pure helium.

The formation frequency of LMXBs fed by helium stars can be estimated from Figure 1 and equation (11) as $\nu_x \sim 5 \times 10^{-4}$ yr^{-1}. The lifetime of such LMXBs can be estimated as $\tau_x \sim M_{\rm He}/3 \times 10^{-8}\ M_\odot\ {\rm yr}^1 \sim 10^7$ yr, so we can estimate the total number of such systems in the Galaxy to be $N_x \sim \nu_x \tau_x \sim 5000$. This number exceeds by two orders of magnitude the number of known bright LMXBs. A possible reason for this apparent discrepancy (which remains even if we have overestimated the occurrence frequency of these systems by a factor of 10) is that the X-ray heating of the helium star causes an increase in the effective mass-transfer rate, forcing the development of a common envelope which increases the rate of orbital shrinkage; the feedback in this process could lead to a runaway situation, drastically reducing the effective lifetime of the system. Alternatively, the common envelope could absorb the X-ray emission and prevent detection of the system as an X-ray source. A similar argument could be applied to systems in which the donor is a hydrogen star; the formalism also predicts far more LMXB stars which are accreting hydrogen than are observed. Another possible explanation is that the phase space associated with the initial mass ratio is not given at all well by the factor dq in equation (11), but then we would have to explain why the same formalism predicts correctly the formation frequency of ordinary cataclysmic systems for which a similar range of q values applies.

2. RESPONSE OF A CO DEGENERATE DWARF TO ACCRETION

For a very wide range of combinations of component masses, orbital shrinkage driven by gravitational wave radiation produces a mass-transfer rate between $2 \times 10^{-8}\ M_\odot$ yr^{-1} and $4 \times 10^{-8}\ M_\odot$ yr^{-1} (Savonije, deKool, & van den Heuvel 1986; Iben & Tutukov 1987; Iben et al. 1987; Tutukov & Fedorova 1989). For simplicity, we have adopted in the present study a constant accretion rate $dM/dt \sim 3 \times 10^{-8}\ M_\odot$ yr^{-1}.

The thermal structure of a model CO white dwarf accreting helium at the rate $3 \times 10^{-8}\ M_\odot$ yr^{-1} is shown for various times in Figure 2. The time elapsed since the beginning of accretion is indicated beside each numbered profile. The initial model, which is not described in Figure 1, is of mass 1.01 $M_\odot$, has a very narrow ($<0.005\ M_\odot$) helium-containing layer near its surface, and derives from a hot configuration approximating the core of the central star of a planetary nebula which has been allowed to cool for $\sim 1.3 \times 10^8$ yr. It is nearly isothermal at a temperature of about 18×10^6 K. Characteristics of several models are presented in Table 1.

Most of the compressional energy which is liberated locally in the interior of a model in consequence of accretion goes locally into increasing the zero-point energy of degenerate electrons (the ratio of Fermi energy ϵ_F to kT in the middle of the model is in the range 10–12). A portion goes into increasing the thermal energy of nondegenerate nuclei (we shall hereinafter call them "ions") and, when temperatures become high enough, a portion is lost in the form of neutrinos. The remainder of the liberated energy flows either inward or outward, the "watershed" occurring at the point of maximum temperature (see Fujimoto et al. 1984 for a discussion of the nature of this phenomenon in the context of an accreting neutron star). Until nuclear burning becomes important, the major contribution to both the inward and outward flow comes from the accreted layer. Until neutrino losses become important (only near the

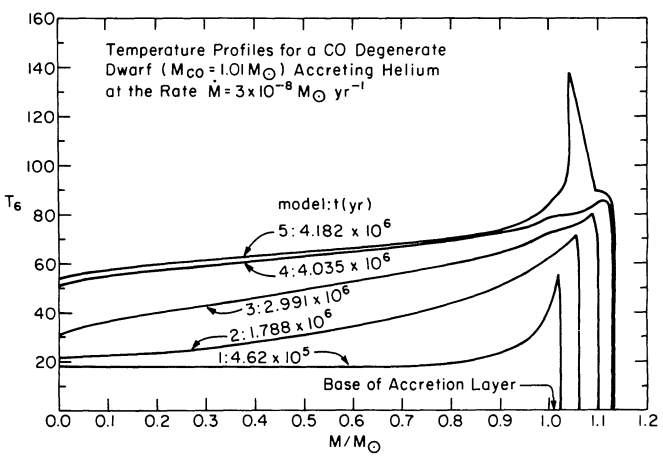

FIG. 2.—Evolution of the temperature profile of a CO degenerate dwarf of initial mass 1.01 $M_\odot$ accreting helium at the rate $3 \times 10^{-8}\ M_\odot$ yr^{-1}. Model numbers are the same as in Table 1.

TABLE 1

PROPERTIES OF A CARBON-OXYGEN DWARF MODEL OF INITIAL MASS 1.01 $M_\odot$ ACCRETING HELIUM AT THE RATE 3×10^{-8} $M_\odot$ yr^{-1}

Model	Time (yr)	Mass (M_0)	Radius (R_0)	Luminosity (L_0)	Central Density (g cm^{-3})	Central Temperature (deg K)	Shell Density (g cm^{-3})	Shell Temperature (deg K)
1.....	4.623/6	1.02387	0.00841	1.500	3.25/7	1.81/7	1.05/5	5.53/7
2.....	1.788/6	1.06344	0.00807	2.454	4.15/7	2.13/7	2.27/5	7.17/7
3.....	2.991/6	1.09975	0.00769	2.937	5.23/7	3.06/7	3.34/5	8.01/7
4.....	4.035/6	1.13500	0.00729	3.320	6.67/7	5.35/7	6.14/5	8.81/7
5.....	4.182/6	1.13529	0.00731	4.960	6.66/7	5.36/7	2.28/6	13.8/7

end of the accretion episode when nuclear burning also becomes important), the major beneficiary of the inward flow is the thermal energy of the ions. On reaching the surface, the outward flow leaves the star as radiation in a blackbody distribution at $\sim$80,000 K.

The rate at which the ionic thermal energy increases ($dU_{\rm ion}/dt$) and the rate at which energy is lost via neutrinos ($-\epsilon_\nu$) are shown in Figures 3*a*–3*d* as functions of position for four of the models whose temperature profiles are given in Figure 2. Rates are in units of ergs g^{-1} s^{-1} and position is described by the mass coordinate in units of $M_\odot$. Shown also in these figures is the position of the watershed ($L = 0$) and the position to the left of which $\epsilon_g < 0$ and to the right of which $\epsilon_g > 0$. Here, $\epsilon_g = -P\,dV/dt - dU/dt$, where $-P\,dV/dt$ is the rate at which the gravitational field does work (rate of release of gravitational potential energy) and dU/dt is the rate of increase of total internal energy. We shall follow the standard convention of referring to ϵ_g as the rate of release of gravitational energy, noting that it is actually the difference between the rate at which gravitational potential energy is released and the rate at which the internal energy is increased. Finally, integrated quantities are given in the upper left corner of each figure: $L_g = \int \epsilon_g\,dM$, $L_\nu = \int \epsilon_\nu\,dM$, $L_n = \int \epsilon_n\,dM$, $dE_{\rm ion}/dt = \int (dU_{\rm ion}/dt)dM$, and $L_s = L_g + L_n + L_\nu$ = surface luminosity. The rate ϵ_n of the liberation of nuclear energy is not shown; it is small in all but the fourth model where it reaches $\epsilon_n \sim 18$ ergs g^{-1} s^{-1} over most of the accreted layer.

The near discontinuity in $dU_{\rm ion}/dt$ at the base of the accreted layer is due to the fact that the mass of a nucleus to the left of the discontinuity is over 3 times larger than the mass of a nucleus to the right of the discontinuity. The discontinuity is actually of width $\sim$0.005 $M_\odot$, as all composition profiles have been artificially spread out over this distance for ease in calculating.

It is particularly interesting that $dE_{\rm ion}/dt$ and L_s are comparable in size during the entire accretion phase, up to the onset of the thermonuclear runaway. Approximately half of the gravitational energy released in consequence of accretion goes into increasing the thermal energy of ions in the interior and the other half is lost from the surface; only a small fraction of the energy released in the accreted layer remains in this layer to heat matter there to sufficiently high temperatures to initiate a

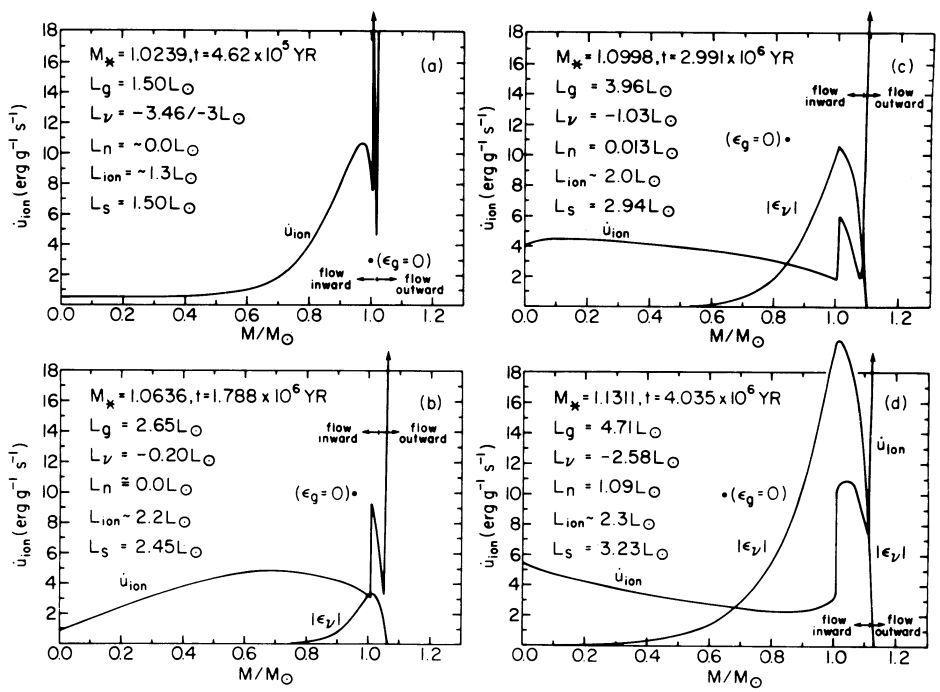

FIG. 3.—(*a*–*d*) Time evolution of the heating rate for the ionic component ($dU_{\rm ion}/dt$) and of the rate of neutrino cooling (ϵ_ν) for the model of initial mass 1.01 $M_\odot$. Global characteristics are given at the left in each panel. The watershed to the left of which energy flows inward and to the right of which it flows outward is indicated, as is the point to the left of which $\epsilon_g < 0$ and to the right of which $\epsilon_g > 0$.

thermonuclear runaway. The bulk of the energy released either flows out of the star or flows inward to heat up the matter throughout the interior of the white dwarf to temperatures comparable with those achieved in the accreted layer.

Figures 3*a–d* show that, as time progresses, the maximum of $dU_{\rm ion}/dt$ in the interior of the degenerate dwarf below the accreted layer moves inward, eventually reaching the center. From the figures one may estimate that the time scale for the diffusion of energy inward is of the order of 10^6 yr, and this may be used to infer qualitatively how the mass of the accreted layer at the onset of the thermonuclear runaway depends on the accretion rate. Suppose, for example, that we choose an accretion rate 10 times larger. The rate at which energy is liberated in the accreted layer is increased by about a factor of 10, but the rate at which energy leaks inward is primarily a function only of the difference between the temperature in the accreted layer and the temperature in the interior. Hence, the rate at which matter in the accreted layer is heated is much larger in the case of more rapid accretion, and temperatures in the accreted layer become high enough to initiate a thermonuclear runaway after much less material has been accumulated than in the smaller dM/dt case. Similarly, if we decrease the accretion rate by a factor of 10 from the standard case, a smaller fraction of the energy released in the accreted layer will remain in the layer and a larger mass will have to be accreted before a thermonuclear runaway can be initiated. As the accretion rate is lowered below some minimum value, such that the temperatures throughout both the accreted layer and the interior CO core increase at nearly the same rate, the critical accreted mass for a thermonuclear runaway will approach some maximum value asymptotically.

Several additional features of model number 4 are shown in Figure 4. The fact that, everywhere below the base of the accreted layer, $-P\,dV/dt$ is over two orders of magnitude larger than either $|\epsilon_g|$ or $dU_{\rm ion}/dt$ (Fig. 3*d*) demonstrates explicitly that almost all of the work done by gravity in the interior goes into raising the kinetic energy of the highly degenerate electrons. This is, of course, already obvious from the fact that a zero temperature electron gas is adiabatic and that departures from adiabaticity are of order $(kT/\epsilon_F)^2$. The energy for the increase in the temperature of the nondegenerate ions comes primarily from the inward flow of energy emerging from the

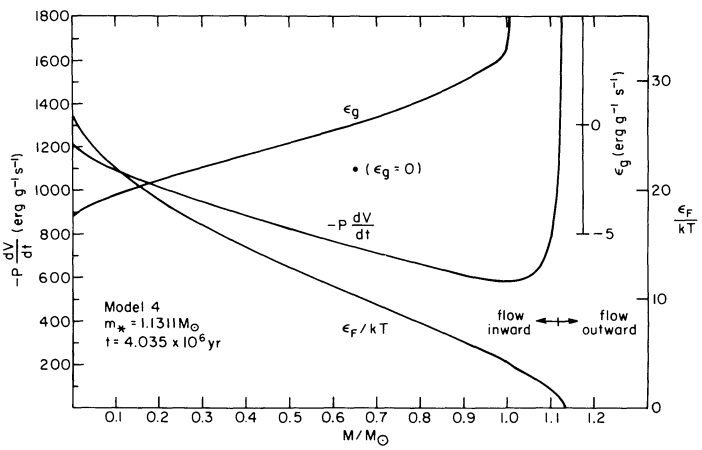

FIG. 4.—The rate of "gravitational energy" generation ϵ_g as a function of position in model 4. The rate of release of gravitational potential energy $-P\,dV/dt$ is shown separately, along with ϵ_F/kT, a standard measure of the degree of degeneracy.

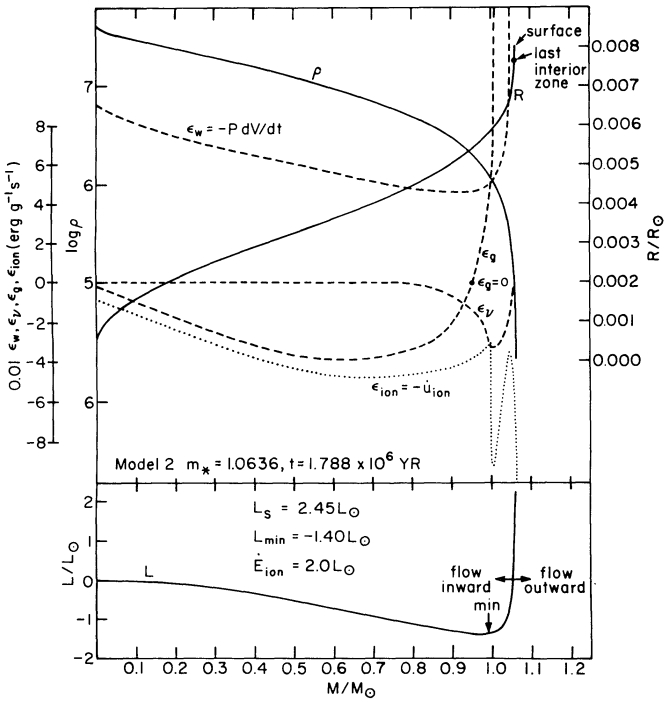

FIG. 5.—Density and radius profiles within model 2 are shown together with the neutrino cooling rate $-\epsilon_\nu$, the ion heating rate $\epsilon_{\rm ion}(=dU_{\rm ion}/dt)$, and the rate at which work is being done by the gravitational field ϵ_w $(=-P\,dV/dt)$. The integral flux (luminosity $L=\int[\epsilon_n+\epsilon_g+\epsilon_\nu]dM$) is shown in the lower panel.

base of the accreted layer rather than from adiabatic compression of the ions. This is illustrated further by the luminosity and ϵ_g curves in Figure 5, where additional characteristics of model 2 are shown. Contributions to the inward flow continue for about 0.06 $M_\odot$ below the base of the accreted layer, but by far the major contribution comes from the accreted layer. The maximum rate of inward flow $(=-L)$ occurs just below the base of the accreted layer and has the value 1.4 $L_\odot$. Inward of this point, the total rate at which the ionic kinetic energy increases is $\sim$1.7 $L_\odot$ and approximately 0.1 $L_\odot$ is used up in neutrino losses. This means that the integral of $-P_{\rm ion}\,dV/dt$ over the body of the original degenerate dwarf is approximately 0.4 $L_\odot$. As time progresses and the temperatures in the accreted shell increase, the importance of compressional heating decreases. Inward flow is by conduction, with electrons near the top of the Fermi sea transferring energy to the ions by inelastic scattering.

Figure 6 shows that the maximum inward flux always occurs very close to the border between the accreted layer and the surface of the original dwarf. Over the entire accretion phase, the average value of this flux is $\sim$1.5 $L_\odot$, and this is comparable with the rate at which ions are being heated interior to the point of minimum luminosity. Thus, almost all of the heating of ions in the matter of the original degenerate dwarf is due to energy flowing inward from this point, and therefore the heating is much more rapid than would be the case under adiabatic compression. This is demonstrated explicitly in Figure 7, where the motion in the ρ-T plane of matter at several mass points is compared with adiabatic paths. At the stellar center, the path is initially adiabatic, as energy has not had time to reach the center from surface layers, but as time progresses, the path departs farther and farther from the adia-

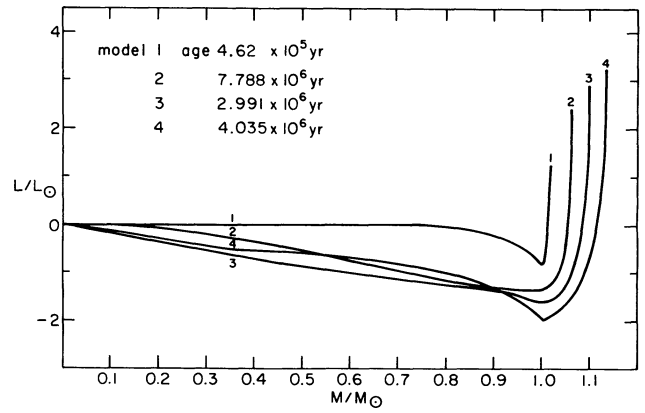

FIG. 6.—Evolution of the luminosity profiles within the accreting degenerate dwarf of initial mass 1.01 $M_\odot$. Model numbers are the same as in Table 1.

batic law. At the mass point 0.9 $M_\odot$, the path is steeper than adiabatic for the first half of the accretion episode, but then becomes less steep than adiabatic when neutrino losses become important. At the mass point 1.0 $M_\odot$, the path remains subadiabatic because energy is being contributed at a high rate to the inward flow.

We have also examined the response of a cold 0.6 $M_\odot$ degenerate dwarf to the accretion of helium at the rate 3×10^{-8} yr^{-1} and find the behavior of the model to be nearly identical with that of the 1.01 $M_\odot$ model. The temperature history of the model is shown in Figure 8. For our purposes in the remainder of this section, it suffices to note that, just as in the case of the more massive dwarf, the rate of increase of ion kinetic energy is comparable with the rate of energy loss from the surface and that the energy for ionic heating in the interior comes primarily from the accreted layer. The mass in the accreted layer when a thermonuclear runaway begins is only slightly larger than in the 1.01 $M_\odot$ case (0.152 $M_\odot$ instead of 0.131 $M_\odot$ [we include the mass of helium at the surface of the initial CO white dwarf]). In the next section, where we discuss the early stages of the thermonuclear runaway, we provide

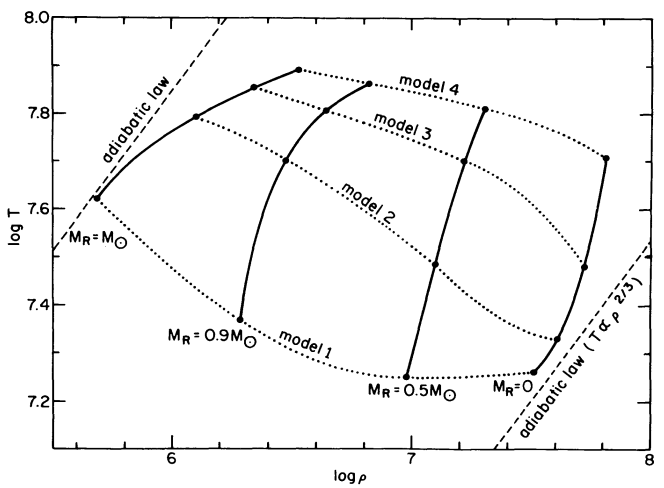

FIG. 7.—The thermal evolution of matter at several Lagrangian mass points within the accreting degenerate dwarf model of initial mass 1.01 $M_\odot$. Adiabatic trajectories are displayed in the lower right-hand and upper left-hand corners. Solid lines join points of common Lagrangian mass and dotted lines give the density-temperature distribution within models numbered according to Table 1.

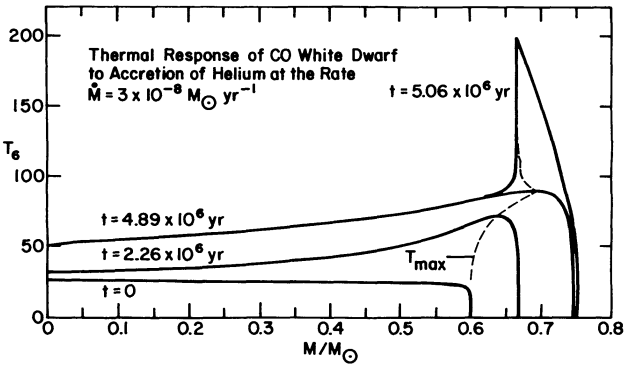

FIG. 8.—Evolution of temperature profiles within the accreting degenerate dwarf of initial mass 0.6 $M_\odot$. Times from the beginning of the accretion phase are indicated beside each profile.

enough details for the reader to make comparisons between interior properties of the two models.

It is possible to explain why the mass of helium which must be accreted before a thermonuclear runaway begins is nearly the same in the two cases. To us, this was initially a very surprising result, as it conflicts with the intuition provided by the classical theory of novae powered by hydrogen burning. In the classical theory, a first-order estimate of the mass of fuel which must be accreted before a thermonuclear runaway occurs can be obtained in a one-zone approximation (Tutukov & Yungelson 1972; Tutukov & Ergma 1979; Ergma & Tutukov 1980). The zone is taken to be the accretion layer, and thermal communication with the interior degenerate dwarf is ignored. The basic structure of the zone is set by assuming at first that there is exact balance between the gravitational energy liberated in the zone and the rate at which energy flows outward through this zone; that is, all of the gravitational energy liberated in the accretion layer is assumed to be eventually radiated from the surface. One may estimate the rate at which nuclear energy is released, and, assuming that the condition for a thermonuclear runaway to begin is that the rate of nuclear energy production just equals the rate of liberation of gravitational energy, an estimate of the critical mass m_e follows. When the accreted fuel is helium, the critical mass of the accreted layer is given by (Iben & Tutukov 1989b):

$$m_e \sim 10^{6.65} R_{\rm CO}^{3.75} M_{\rm CO}^{-0.3} (dM/dt)_{-8}^{-0.57} , \qquad (13)$$

where $R_{\rm CO}$ is the radius of the degenerate dwarf in solar units, $M_{\rm CO}$ is the mass of this dwarf in solar units, and $(dM/dt)_{-8}$ is the mass-accretion rate in units of 10^{-8} $M_\odot$ yr^{-1}. Curve A in Figure 9 shows how the value of m_e predicted by equation (13) varies with $M_{\rm CO}$. The filled stars describe our model results, the filled circle is from Nomoto (1982a), and the open circle is from Taam (1980a). It is evident that the assumptions made in constructing the simple one-zone model do not apply to the case of the accretion of helium onto a cold degenerate dwarf.

The basic reason for the failure of the simple model is that the initial degenerate dwarf is cold and electron conductivity is high. In an earlier study (Iben & Tutukov 1985) involving the accretion of hydrogen onto a cold low-mass degenerate dwarf, we found that the inward flux exceeded the outward flux by a factor of ~ 10. Our experiments here demonstrate that most of the energy liberated in the accretion layer flows either into the interior or to the surface. The temperatures in the accretion layer are tied to those in the interior by the high conductivity; helium ignition temperatures cannot be reached until the inte-

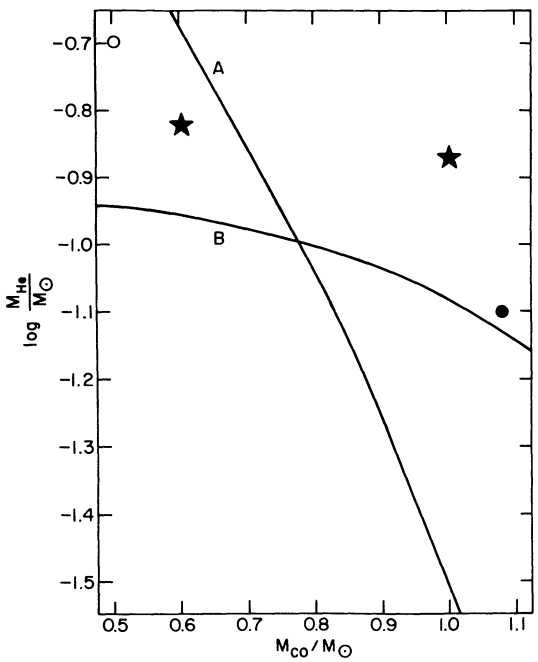

FIG. 9.—The mass of accreted helium at the start of a thermonuclear runaway as a function of the initial mass of the accreting CO degenerate dwarf. The accretion rate is 3×10^{-8} yr^{-1}. The open circle in the upper left-hand corner is interpolated from the results of Taam (1980a) and the filled circle just above the curve labeled B is from Nomoto (1982a). Curve A is defined by eq. (13) in the text and curve B follows from eq. (17) with $\beta = \frac{1}{2}$ and $T_8 = 1$. The solid stars are from our two experiments described in this paper.

rior has been heated up to temperatures comparable with those in the accreted layer.

Mindful of these results, we construct a simple two-zone model, assuming that a fraction β of all of the gravitational energy liberated in the outer zone (the accreted layer) is absorbed by the nondegenerate ions in the inner zone (the original degenerate dwarf). The mean density ρ of the accreted layer may be defined by

$$m_e \sim 4\pi\rho h R_{\rm CO}^2 , \quad (14)$$

where h is the thickness and $R_{\rm CO}$ is the mean radius of the accreted layer. The condition for hydrostatic equilibrium is

$$GM_{\rm CO} m_e/4\pi R_{\rm CO}^4 \sim P_e \sim 10^{13}(\rho/\mu_e)^{5/3} , \quad (15)$$

where G is the gravitational constant, P_e is the average pressure of degenerate electrons, and μ_e is the electron molecular weight. The final equation is that of energy conservation:

$$\beta(GM_{\rm CO}/R_{\rm CO}^2)h \int (dM/dt)dt = \beta G(M_{\rm CO}/R_{\rm CO})^2 h m_e \sim 3/2(kT/\mu_{\rm ion} M_{\rm H})M_{\rm CO} , \quad (16)$$

where we have assumed that a fraction β of all of the gravitational energy released in the process of shell compression goes into heating the ions in the interior to an average temperature T. Here k is the Boltzmann's constant, $\mu_{\rm ion}$ is the average ion molecular weight in the interior, and $M_{\rm H}$ is the mass of the hydrogen atom.

Combining equations (14)–(16) gives

$$m_e \sim 0.065\beta^{-5/7} r_{\rm CO}^{8/7} M_{\rm CO}^{3/7} T_8^{5/7} , \quad (17)$$

where $r_{\rm CO}$ is the CO degenerate dwarf radius in units of 10^{-2} $R_\odot$ and T_8 is the helium ignition temperature in units of 10^8 K. The criterion for a helium-burning runaway to begin is still that the rate of nuclear energy generation approximately equals the rate of energy loss from the surface, which we can take to be (1-β) times the rate of release of gravitational energy in the accreted layer. The rate of energy generation by the triple-α process depends so sensitively on the temperature (approximately as the 40th power) that it suffices to set $T_8 \sim 1$. Finally, setting $\beta = \frac{1}{2}$, curve B in Figure 9 results.

The predicted critical mass of the accreted layer depends only weakly on the CO dwarf mass and does not depend at all, in this approximation, explicitly on the accretion rate. The slope of curve B corresponds well with that defined by our two experiments. The difference in absolute value between the model results and the analytic results can be understood qualitatively as a consequence of the neglect of neutrino losses in the simple model; including these losses leaves less energy for heating ions in the interior, corresponding to a smaller β or to the accretion of more mass before ignition temperatures are reached.

The difference between the Nomoto (1982a) result and our results can be ascribed to a typographical error on page 545 of a paper by Iben (1975). As has been pointed out in several subsequent papers, the quantity α used in equations (A13)–(A21) on page 545, where an analytic approximation to the conductivity is defined, should be $\alpha = 2 \times \log(\langle\lambda/2R\rangle)$ instead of $\alpha = 1 \times \log(\langle\lambda/2R\rangle)$. The use of a smaller α has the effect of decreasing the conductivity. A smaller conductivity means that more energy is bottled up in the accreted layer relative to what can diffuse into the interior or, equivalently, to a smaller portion of the CO dwarf that experiences ionic heating due to the flux of energy from the accretion layer; a smaller effective mass at a fixed dwarf radius in equation (17) means a smaller critical mass for the accreted layer. This explains why Nomoto's critical accreted mass is smaller than ours by a factor of ~ 1.7.

3. THE THERMAL RUNAWAY AND ITS CONSEQUENCES—SUPER NOVA OR DWARF SUPERNOVA?

Properties of the outer layer of the 1.01 $M_\odot$ accreting dwarf and of the accreted layer are shown in Figure 10 at a time when the rate of nuclear energy generation and the rate of neutrino losses have become comparable with the surface luminosity. Note that the minimum of luminosity occurs very near the base of the accreted layer and that the rate of influx there (1.4 $L_\odot$) is quite similar to that at the base of the accreted layer in the 0.6 $M_\odot$ model at a similar stage (see Fig. 12). Some nuclear energy is being liberated near the outer edge of the original degenerate dwarf because of a small residue of helium in the initial model; due to the large abundance of carbon, this helium burns primarily through the ^{12}C(α, γ)^{16}O reaction. The opacity and the radiative component of the opacity are shown in the lower panel of Figure 10 to illustrate the high conductivity which is responsible for transferring energy from the base of the accreted layer into the interior.

Figure 11 shows properties of the same model when the rate of release of nuclear energy has exceeded by a factor of about 3 the rate of energy loss from the surface. It is evident that a thermonuclear runaway is in progress. Figures 12 and 13 show conditions in the accreted layer of the more massive model at stages similar to the stages of the less massive model described in Figures 9 and 10.

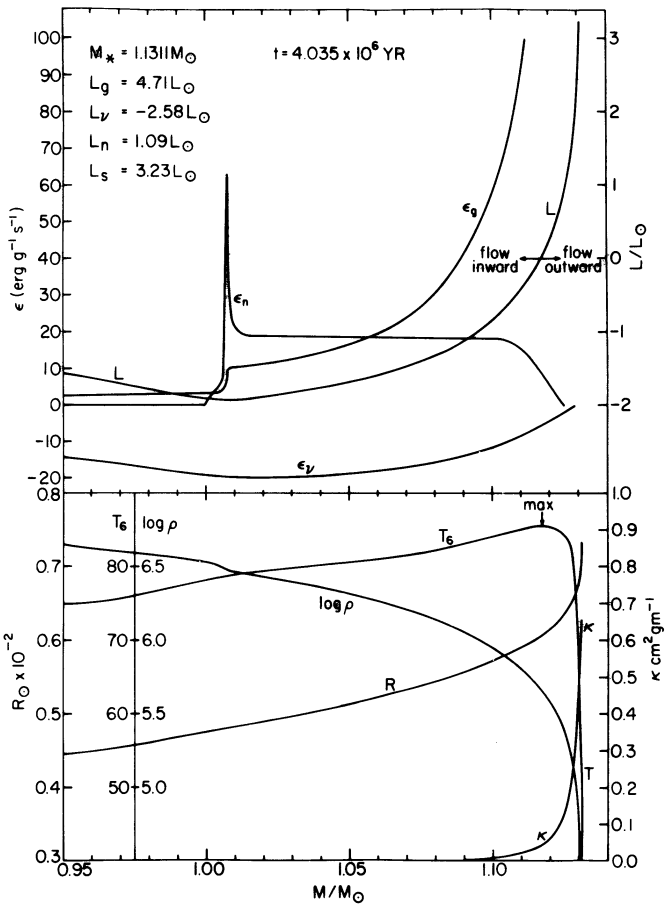

FIG. 10.—Characteristics in the outer part of the accreting CO degenerate dwarf of initial mass 1.01 $M_\odot$ when the integrated rate of nuclear energy generation L_n has begun to become comparable with the surface luminosity L_s. The main global parameters of the model (model 4 in Table 1) are shown in the upper left-hand corner of the upper panel. In the upper panel are shown distributions of the local rate of gravitational energy release ϵ_g, integral energy flux L, and the local rate of nuclear energy generation ϵ_n. Distributions of temperature T_6 (in units of 10^6 K), density ρ, radius R, and opacity κ are presented in the lower panel.

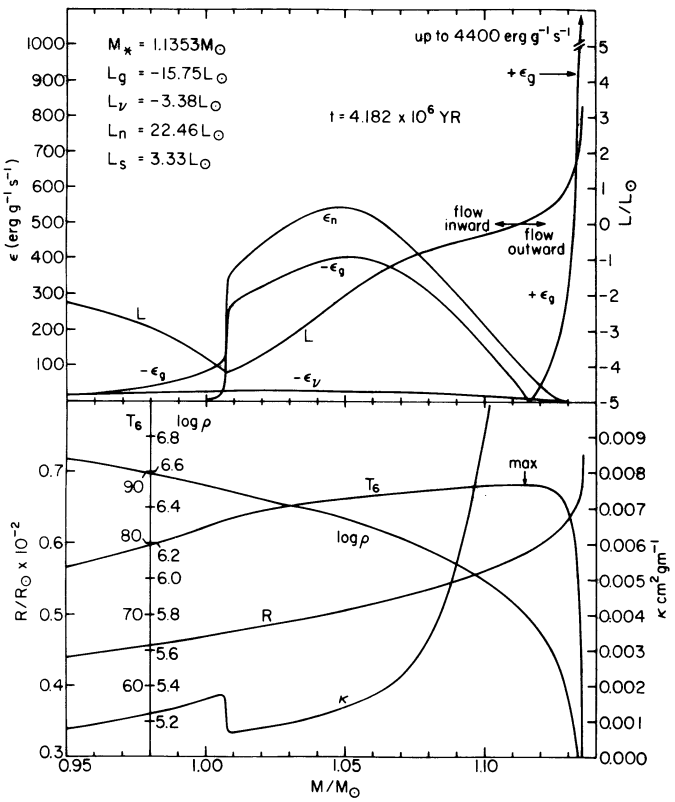

FIG. 11.—Same as Fig. 10 for model number 5 of the accreting CO degenerate dwarf of initial mass 1.01 $M_\odot$ when the nuclear-burning luminosity substantially exceeds the surface luminosity.

Computations were stopped in the low mass case when the helium-burning luminosity reached $L_n = 5 \times 10^9\ L_\odot$ and in the high mass case when $L_n = 5 \times 10^9\ L_\odot$. The density and temperature structures of the final models are shown in Figure 14, along with several lines of constant ϵ_F/kT and a line labeled "degeneracy border" which has been constructed by setting $P_{e,\mathrm{deg}} \sim 10^{13}(\rho/\mu_e)^{5/3} = P_{e,\mathrm{nondeg}} = \rho kT/\mu_e M_H$. In the final models, convection extends outward from the point of maximum temperature by about 350 km and the convective shell contains a mass of about 0.05 $M_\odot$; convective velocities are about 3 km s^{-1}. At this point, evolution is accelerating so rapidly that the approximation of a constant entropy in the convective shell is beginning to break down. Calculations were therefore terminated.

The outcome of the ensuing explosion in each case can be understood from an examination of the degree of electron degeneracy in the accreted layer at the onset of the thermonuclear runaway. The larger the degree of degeneracy, the more dramatic are the consequences. Several investigators (Ergma, Rahunen, & Vilhu 1978; Fujimoto 1980; Nomoto 1980, 1982a, b, 1984; Taam 1980a, b; Fijimoto & Sugimoto 1982; and Khokhlov 1990) have concluded that whether the thermonuclear runaway is mild (as in a classical nova explosion) or whether it develops into a deflagration or detonation (which incinerates matter in the outer half of the accreted shell and possibly also in the entire star) is a relatively well-defined function of the mass accretion rate and of the CO degenerate dwarf mass, with 2–5 $\times 10^{-8}\ M_\odot\ \mathrm{yr}^{-1}$ being a critical accretion rate which separates the response to ignition into two types—nova-like or supernova-like (see Iben & Tutukov 1984b for a discussion of this theme). Our results show that, the smaller the mass, the smaller must be the accretion rate for incineration to occur.

When the accretion rate is fixed, as in the current case, the outcome of ignition depends only on the mass of the degenerate dwarf core. In the case of accretion onto the model of initial mass $M_{CO} = 1.01$, the situation is very clear-cut. The thermal runaway is initiated at a point where $\rho \sim 2 \times 10^6$ g cm^{-3}, $T \sim 8 \times 10^7$ K, and $\epsilon_F/kT \sim 25$. An increase in pressure sufficient to cause expansion cannot occur until the temperature has increased to more than 10^9 K (close to the degeneracy border in Fig. 14). The time scale for the complete conversion of helium into carbon (neglecting all reactions other than the triple-α reaction) is

$$\tau_{3\alpha}\ (\mathrm{s}) \sim X_4^{-3} T_8^3 \rho_6^{-2} \exp\left(-14.33 + 43.20/T_8\right), \quad (18)$$

where T_8 and ρ_6 are the temperature and density in units of 10^8 K and 10^6 g cm^{-3}, respectively, and X_4 is the abundance by mass of ^{4}He. The time scale for dynamical expansion of the shell may be approximated by (Taam 1980a, b)

$$\tau_{\mathrm{dyn}} = (24\pi G\rho)^{-1/2} = 0.32\ \mathrm{s}\ (2 \times 10^6\ \mathrm{g\ cm}^{-3}/\rho)^{1/2}. \quad (19)$$

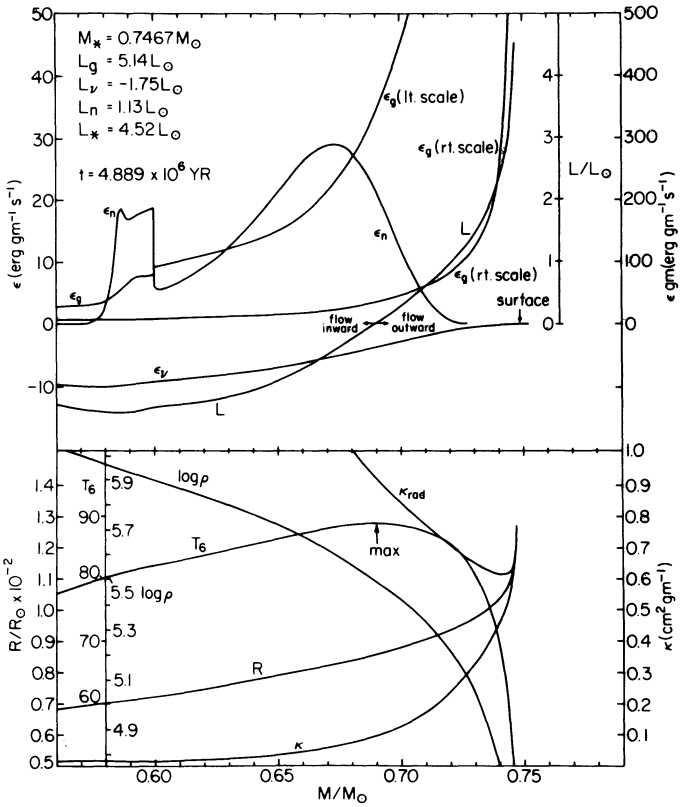

FIG. 12.—Characteristics in the outer part of the accreting CO degenerate dwarf of initial mass 0.6 $M_\odot$ when the integrated rate of nuclear energy generation L_n has begun to become comparable with the surface luminosity L_s. The main global parameters of the model are shown in the upper left-hand corner of the upper panel. In the upper panel are shown distributions of the local rate of gravitational energy release ϵ_g, integral energy flux L, and the local rate of nuclear energy generation ϵ_n. Distributions of temperature T_6 (in units of 10^6 K), density ρ, radius R, and opacity κ are presented in the lower panel.

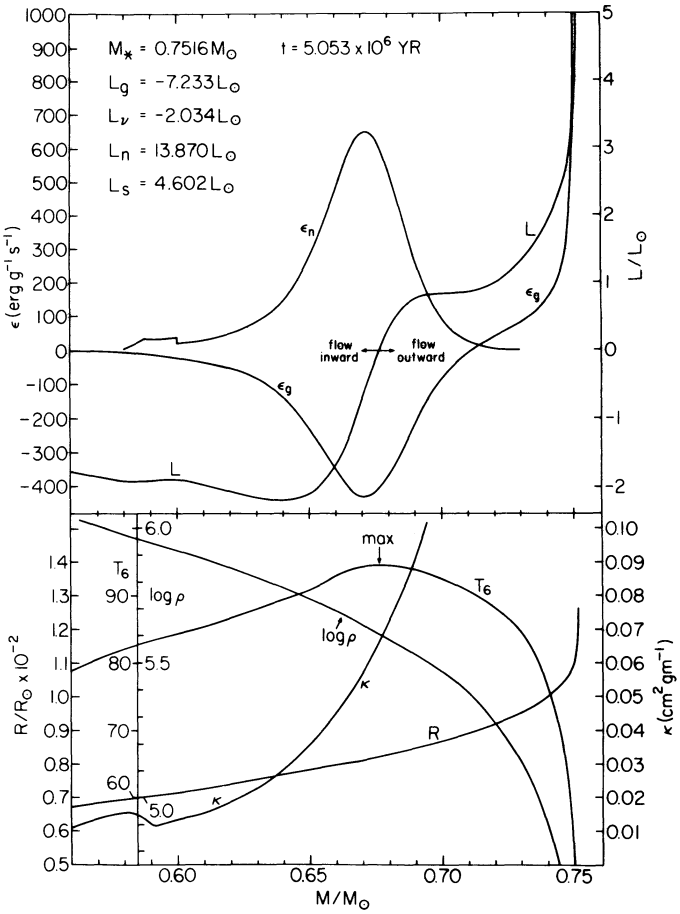

FIG. 13.—Same as Fig. 12 for the accreting CO degenerate dwarf of initial mass 0.6 $M_\odot$ when the nuclear-burning luminosity substantially exceeds the surface luminosity.

At $\rho_6 = 2$ and $T_8 \sim 4.4$, $\tau_{3\alpha} \sim \tau_{\rm dyn} \sim 0.3$ s and it is clear that, long before the degeneracy border is reached, all of the helium will have burned up and nuclear processing will have continued until iron-peak nuclei have been produced in statistical equilibrium. The amount of energy per gram released in the conversion of ^{4}He into ^{12}C is 6×10^{17} ergs and the additional energy released in going all the way to statistical equilibrium is 8×10^{17} ergs. If all of the energy released were to go into thermal motions, this is sufficient to increase the temperature to about 2×10^{10} K. However, once $kT > \epsilon_F$, the overpressure is large enough to ensure that dynamical expansion must occur. If all of the nuclear energy released were converted into the kinetic energy of the expanding material, the velocity of this material would be about $v_{\rm max} \sim 1.7 \times 10^4$ km s^{-1}. However, some fraction of the nuclear energy released must be used up in overcoming the gravitational binding energy. The binding energy per gram of the accreted layer is about

$$GM_{\rm CO}/R_{\rm CO} \sim 1.8 \times 10^{17} \text{ ergs g}^{-1}\,, \qquad (20)$$

or about 10% of the total nuclear energy released.

Too much energy is released too rapidly for the star to respond other than by developing shocks that are driven by the energy released. A flame front proceeds outward, imparting greater than escape velocity to all matter left behind (Nomoto 1982b; Khokhlov 1990). It is not clear that a flame front also proceeds inward; Nomoto finds that it may, but Khokhlov finds that it does not. In either case, the model explodes as a supernova, mild if only part of the accreted layer is incinerated and expelled (hence the term "dwarf" supernova), but of standard power if the entire star is incinerated.

The situation is also fairly clear-cut when $M_{\rm CO} = 0.6$ (see Fig. 14). The thermonuclear runaway begins at a point where $\rho \sim 4 \times 10^5$ g cm^{-3} and $T \sim 8 \times 10^7$ K, precisely the density and temperature which prevail at the onset of the thermal runaway in the electron-degenerate helium core of a low-mass red giant (Despain 1981; Mengel & Sweigart 1981). In the low-mass red giant, the runaway does not develop into a hydrodynamic event (Fujimoto, Iben, & Hollowell 1990) and it is reasonable to suppose that the development of the helium flash in the case of the accreting low mass white dwarf will also be of a quasi-static character. In both cases, $\epsilon_F/kT \sim 10$ when ignition occurs and, in the case of the helium core flash, expansion due to an increase in pressure limits the temperature increase to $\sim 3 \times 10^8$ K.

In the case of the accreting low mass white dwarf, all matter above that which participates in the thermonuclear runaway (which begins at about the middle of the accreted layer) expands beyond the enveloping Roche lobe and is presumably lost from the system. If the escaping matter experiences a strong frictional interaction with the orbiting stellar com-

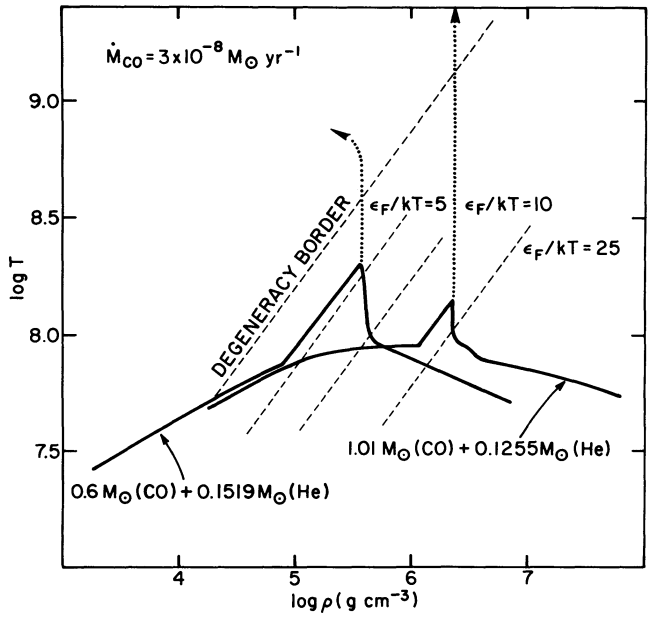

FIG. 14.—Characteristics in the density-temperature plane of CO degenerate dwarfs accreting helium at the onset of helium-burning thermonuclear runaways. The solid curves describe the last two models computed for the models of initial masses 0.6 $M_\odot$ and 1.01 $M_\odot$. Several lines of constant ϵ_F/kT are shown, and the degeneracy border is defined by $P_{e,\mathrm{deg}} \sim 10^{13}(\rho/\mu_e)^{5/3} = P_{e,\mathrm{nondeg}} = \rho kT/\mu_e M_H$. The dotted lines give the anticipated trajectories of the point of maximum temperature as the thermonuclear runaway progresses.

ponents, these components may be forced closer together to such an extent that a merger ensues. In this event, the system will evolve into an R CrB star surrounded by an expanding shell of helium. On the other hand, the amount of mass lost in the outburst is small compared with the mass of the remnant system, and the net result may be orbital expansion (see § 6). In this event, the system will survive as a binary, as in the case of classical nova events.

If the analogy with core helium-burning flashes in low mass red giants were to persist, we might expect that several more flashes will occur, each being initiated closer to the base of the layer of accreted helium that still remains, and each resulting in an expansion beyond the Roche lobe and mass loss from the system, until most of the mass that was accreted prior to the initial outburst has been lost from the system. The mass of helium-rich material remaining after the last outburst can be estimated from models of AGB stars. For example, the model of core mass $M_{CO} = 0.6$ will shrink within its Roche lobe once the mass of helium-rich matter remaining above the CO core decreases below $\sim 0.02\ M_\odot$. The model will continue to shrink, evolving to the blue at high luminosity, much as does the central star of a planetary nebula powered by hydrogen burning.

If the expansion velocities of the ejected matter were of the order of those found in ordinary planetary nebulae (10–20 km s^{-1}), the system would survive as a planetary nebula for a time of the order of 10^4 yr. However, expansion velocities will be nearer to the orbital velocities of the stellar components (~ 1000 km s^{-1}) so the nebula may remain detectable for only several hundreds of years. Several additional features distinguish the system from a typical planetary nebula: the most prominent emission features are due to helium recombination rather than to hydrogen recombination; the bolometric luminosity of the system is larger than that of the classical nova produced by a hydrogen-accreting degenerate dwarf of comparable mass, and the mass in the nova shell is from three to four orders of magnitude larger. Hence the term super nova. Outbursts of the predicted type are expected to occur approximately once every century.

When the helium-burning runaway begins, the mass of the accreted layer is much smaller than the core of a red giant when helium is ignited in it, and the mass of the accreted layer is reduced by approximately a factor of 2 in consequence of expansion beyond the surrounding Roche lobe. Hence, the pressures in the remnant accreted layer are much smaller than in the remnant degenerate core of a red giant after the first core flash so that the supposition of multiple flashes in the accretion case may be incorrect. The first flash may evolve into a quiescent helium-burning phase, or helium burning in the remnant of the accreted layer may simply cease. If the first of these eventualities is realized, the system will still evolve into a dwarf supernova; if the second eventuality is realized, the central star of the planetary nebula will be relatively dim and the super nova appellation is inappropriate.

To summarize, helium star cataclysmics in which the accreting white dwarf is massive (say, $M_{CO} > 0.8\ M_\odot$ [see Khokhlov 1990]) probably evolve into dwarf supernovae (possibly accounting for some fraction of all Type Ib supernovae), whereas those in which the accreting white dwarf is of low mass will experience at least one super nova outburst. These latter systems may evolve into R CrB stars or experience several additional outbursts.

4. NEUTRON-CAPTURE NUCLEOSYNTHESIS

Temperatures and densities large enough to cause the conversion of helium into carbon are also large enough to cause the conversion of ^{14}N into ^{22}Ne. In AGB stars of large core mass and in the helium star cataclysmics discussed here, they are also sufficient to induce the reaction ^{22}Ne(α, n)^{25}Mg. In these situations which lead to supernova explosions, the distribution of neutron-rich isotopes formed by neutron-capture nucleosynthesis will definitely not resemble the solar system s-process distribution and in fact might produce r-process isotopes instead. In recurrent helium-star cataclysmics, however, charged-particle nucleosynthesis will stop far short of the production of iron-peak elements and some form of an s-process distribution built on ^{56}Fe as a seed will be produced (Iben 1981); not much thought has been expended in assessing how closely this distribution might resemble the solar system distribution.

It is possible that recurrent helium-star cataclysmics may be responsible for a significant production of heavy neutron-rich isotopes, but it is not clear how large their contribution will be relative to that of low-mass AGB stars. In a solar system distribution, the number of Fe nuclei N_{Fe} is related to the total number of nucleons N_{nucleons} by

$$N_{Fe} \sim 1.2 \times 10^{-5} N_{\mathrm{nucleons}} . \quad (21)$$

An estimate of the rate of production of s-process nuclei by helium-star cataclysmics is given by

$$dN_s/dt \sim 1.2 \times 10^{-5}\ ([0.15\ M_\odot]/M_H) \times \nu_{\mathrm{HeCV}} , \quad (22)$$

where N_s is the number of s-process nuclei, M_H is the mass of a hydrogen atom, and ν_{HeCV} is the formation frequency of recurrent HeCVs. The rate of formation of ^{56}Fe may be estimated as

$$dN_{Fe}/dt \sim (M_\odot/[56\ M_H]) \times \nu_{\mathrm{SNIa}} , \quad (23)$$

where $\nu_{\rm SNIa}$ is the Type Ia supernova rate (most iron is probably produced by Type Ia supernovae which convert a solar mass of material into iron-peak elements). Altogether, then,

$$dN_s/dN_{\rm Fe} \sim 10^{-4} \times (\nu_{\rm HeCV}/\nu_{\rm SNIa}) . \quad (24)$$

Using $\nu_{\rm HeCV} \sim 10^{-2}$ yr^{-1} and $\nu_{\rm SNIa} \sim 3 \times 10^{-3}$ yr^{-1} (van den Bergh, McClure, & Evans 1987), $dN_s/dN_{\rm Fe} \sim 3 \times 10^{-4}$. Since the current ratio of s-process isotopes to iron is about 10^{-3}, our choice of frequencies suggests that HeCVs could account for up to 30% of the s-process isotopes in the Galaxy. Further considerations suggest that this is possibly a considerable overestimate.

Equation (22) supposes that only 0.15 $M_\odot$ of matter is ejected in the entire lifetime of the system. We have argued that some systems may experience many flashes, each being less violent than the previous one, so that the total amount of mass expelled per average system may be as large as 0.3 $M_\odot$. Further, the systems that develop into dwarf supernovae will eject matter which has experienced much higher temperatures than those which develop nova-like outbursts. This means much larger neutron densities during the neutron-capture nucleosynthesis phase. The resulting distribution of neutron-rich isotopes ejected by these systems may therefore resemble an r-process distribution. But, since only 20% of all HeCVs is expected to contain a CO dwarf more massive than $\sim$0.8 $M_\odot$, the contribution to the overall Galactic nucleosynthesis of r-process isotopes will be small.

The fact that the distribution of s-process elements at the surfaces of most stars where their abundances can be estimated is approximately in the solar-system distribution, coupled with the fact that the distribution of neutron-rich isotopes produced by HeCVs is far from being in the solar-system distribution, might be taken as evidence that our estimate of a 30% contribution is far too high. The theory of AGB evolution (e.g., Hollowell & Iben 1988, 1989), coupled with detailed nucleosynthesis calculations in the context of the AGB models (Gallino et al. 1988; Käppeler et al. 1990) tells us that low mass AGB stars produce and bring to their surfaces s-process isotopes in the solar system distribution. The observations (Smith & Lambert 1986; Lambert 1989) tell the same story. AGB stars are formed at the approximate rate of 0.5 yr^{-1} and they eject, either in the form of an ordinary wind or in the form of a nebular shell, enough s-process–enriched matter to account for the bulk of the s-process isotopes in the Galaxy. The rate of production of s-process isotopes by AGB stars may be estimated as

$$dN_s/dt \sim 1.2 \times 10^{-5} \times (f \times 0.1\ M_\odot/M_{\rm H}) \times \nu_{\rm AGB} , \quad (25)$$

where typically 0.1 $M_\odot$ of material in a low-mass AGB star experiences helium burning and a fraction f of processed material is dredged up and lost from the star. This gives

$$dN_s/dN_{\rm Fe} \sim 7 \times 10^{-5} \times f \times (\nu_{\rm AGB}/\nu_{\rm SNIa}) . \quad (26)$$

With $\nu_{\rm AGB} \sim 0.5$ yr^{-1} and $\nu_{\rm SNIa} \sim 3 \times 10^{-3}$ yr^{-1}, it is evident that a dredge-up efficiency of $f \sim 0.1$ is sufficient to account for the observed abundance of s-process isotopes.

5. PROPERTIES OF HELIUM CVS DURING QUIESCENCE

The gross characteristics of helium-star cataclysmics during the quiescent accretion phase can be described. The rate of energy release from the accretion disk is approximately

$$L_{\rm disk} \sim (GM_{\rm CO}/R_{\rm CO})dM/dt \sim 100\ L_\odot\ m_{\rm CO}/r_{\rm CO} , \quad (27)$$

where $m_{\rm CO}$ is the mass of the accretor in solar units and $r_{\rm CO}$ is its radius in units of $10^{-2}\ R_\odot$. The "temperature" of the disk is roughly

$$T_{\rm disk} \sim 48{,}000\ {\rm K}\ M_{\rm He}^{-3/8} m_{\rm CO}^{1/4}/r_{\rm CO}^{-3/4} . \quad (28)$$

The helium star itself has a luminosity (Iben 1990)

$$L_{\rm He} \sim 256\ L_\odot\ M_{\rm He}^{3.676} \quad (29)$$

and a surface temperature

$$T_e \sim 50{,}000\ {\rm K}\ M_{\rm He}^{0.44} . \quad (30)$$

The orbital period is given roughly by

$$P_{\rm orb}\ ({\rm hr}) \sim M_{\rm He}(M_{\rm He} + M_{\rm CO})^{0.16} . \quad (31)$$

These results have all been predicated on an assumed mass transfer rate of $3 \times 10^{-8}\ M_\odot$ yr^{-1}. In reality, the mass-loss rate depends on the mass ratio of components and on the response of the helium-star donor to mass loss. Numerical calculations show that the mass-exchange phase consists of two parts, as described by the solid track in Figure 15 (Tutukov & Federova 1989). During the first part, the mass-exchange rate is almost constant and nearly equal to the one we have assumed. The orbital period decreases in about 10^7 yr to $\sim$13 minutes and the mass of the donor decreases to $\sim$0.2 $M_\odot$. By this time the donor has evolved into a semidegenerate dwarf and, during the second part of the mass transfer phase, the donor loses mass over a period of several times 10^8 yr at a continuously decreasing rate. The orbital period increases to about 40 minutes. An average mass-exchange rate during this phase is $\sim 10^{-9}\ M_\odot$ yr^{-1}. The luminosity of the donor helium dwarf is below 1 $L_\odot$, but the accretion disk luminosity remains at about 3 $L_\odot$.

The very high effective temperatures of the accretion disk and of the helium dwarf itself make the observational detection of systems which are in the slower accretion phase, with an

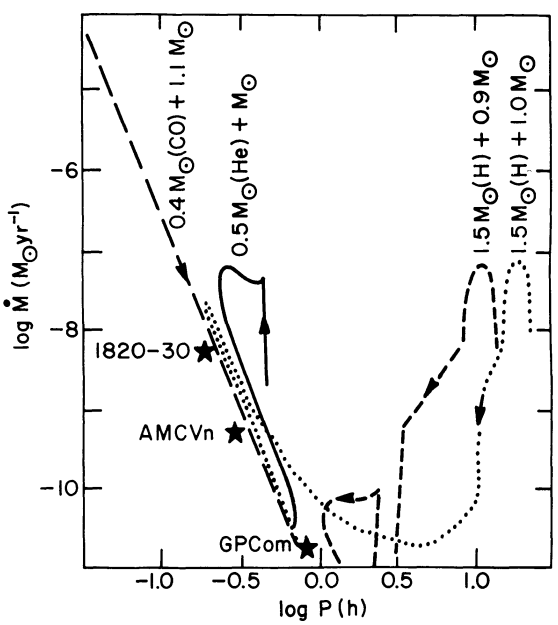

FIG. 15.—Positions of three short-period cataclysmics in the mass exchange rate–orbital period plane. Descriptions of the model trajectories (Tutukov & Fedorova 1989) are given in the text.

apparent visual brightness larger than ~ 10 mag, quite difficult. Thus the detection strategy for hunting for such systems in the solar neighborhood should focus on their expected photometric and spectroscopic periodic variations.

Supposing, as estimated in the first section, that the birth rate of helium star cataclysmics is approximately 10^{-2} yr^{-1} in the entire galaxy, equation (6) suggests that there should be of the order of 10^5 potential HeCVs at any one time and 10^5 HeCVs accreting at the rate $dM/dt \sim 3 \times 10^{-8}\ M_\odot$ yr^{-1}. Figure 15 suggests there should be about 3×10^6 HeCVs accreting at the rate $\sim 10^{-9}\ M_\odot$ yr^{-1}. These numbers correspond to several bright HeCVs and about 100 dim HeCVs within a sphere of radius 100 pc about the Sun. These systems must be tightly concentrated to the disk of the Galaxy since the minimum primary progenitor mass is $\sim 2.5\ M_\odot$.

It is of interest to compare several characteristics of bright HeCVs with those of classical CVs which are in the short-period regime where mass transfer is probably driven primarily by gravitational wave radiation at a rate $(dM/dt)_{\rm HCV} \sim 10^{-10}\ M_\odot$ yr^{-1} (e.g., Paczyński 1967; Faulkner 1971; Tutukov & Yungelson 1979; Iben & Tutukov 1984c). Mass-transfer rates are related by $(dM/dt)_{\rm HeCV}/(dM/dt)_{\rm H} \sim 300$ and lifetimes of the two classes of cataclysmic variables are related by $\tau_{\rm HeCV}/\tau_{\rm HCV} \sim 1/200$.

The mass-exchange process in HeCVs is itself worth a special study. Instabilities in the accretion disk about the accreting white dwarf may occur and provide insight into the physics of disks beyond that obtained by studying only normal CVs. Therefore a numerical study of the stability problem as accomplished by Meyer (1986) for normal CVs is necessary also for HeCVs. Indeed, Smak (1983) has already made a preliminary study, estimating that, for accretion rates in the range 10^{-12}–$10^{-9.1}$ $(P_{\rm orb}/15\ {\rm minutes})^2$, helium disks will be unstable. It is quite probable, therefore, that helium disks with $dM/dt \sim 3 \times 10^{-8}\ M_\odot$ yr^{-1} are stable, both because of the high mass transfer rate and because of the opacity properties of helium as compared with those of hydrogen, and flashes like those occurring in dwarf novae may be absent. On the other hand, when the mass-transfer rate drops to 10^{-9}–$10^{-12}\ M_\odot$ yr^{-1}, which is comparable to the mass-exchange rate in ordinary short-period cataclysmics, dwarf nova-like activity may occur, making the detectability problem less severe.

6. SYSTEM RESPONSE TO THERMAL FLASHES AND FINAL SYSTEM FATE

If there were no interaction between the orbiting stars and the matter escaping the binary system and if the angular momentum per unit mass carried off by the escaping matter were identical with the angular momentum per unit mass of matter in the interior of the mass-ejecting star, then the orbital separation would increase according to the law

$$dA/A = dM/M\ , \tag{32}$$

where dM is the amount of matter lost and M is the total mass of the system. In the case of the $0.6\ M_\odot$ accretor this amounts to a fractional increase in orbital separation of about $dA/A \sim 0.15/(0.75 + 0.4) \sim 0.13$.

Following each outburst, gravitational wave radiation acts to reduce the orbital separation until the helium star again fills its Roche lobe. If gravitational wave radiation alone were responsible for abstracting orbital angular momentum, the time which elapses before Roche-lobe contact is reestablished would be given by

$$\delta\tau_{\rm recontact} \sim \tau_{\rm GW}\, 4\, dA/A \sim 0.5\tau_{\rm GW} \sim {\rm few} \times 10^6\ {\rm yr}\ . \tag{33}$$

However, frictional interaction between the stellar cores and the common envelope could reduce this time substantially.

Once the helium star is forced again into Roche-lobe contact, accretion onto the degenerate dwarf component resumes at the standard rate. This time, however, the degenerate dwarf is hot and much less mass must be accreted before a thermonuclear runaway is initiated. In fact, with each successive flash, the mean temperature of the degenerate dwarf will increase until an approximate steady-state value is reached. Expression (13) should then provide a reasonable approximation to the critical mass of the accreted layer. A typical low mass system may experience two or three outburst episodes before the donor mass decreases below $\sim 0.2\ M_\odot$, at which point the accretion rate decreases below $\sim 10^{-9}\ M_\odot$ yr^{-1} and no further flashes are to be expected.

Following each outburst, once it has contracted within its Roche lobe, the sometimes accretor continues to burn helium at high luminosity for a period of $\sim 10^4$ yr, causing the ejected helium-rich shell to fluoresce as a planetary nebula. However, at an estimated production rate of less than $\sim 3 \times 10^{-2}$ yr^{-1} (assuming about three outbursts per helium star cataclysmic), compared with a formation rate of ~ 0.5 yr^{-1} for ordinary planetary nebulae, at most only one out of 20 or so planetary nebulae can be of this origin and variety. This ratio is probably a very large overestimate since the expansion velocity of the ejected helium envelope is expected to be much larger than that of ordinary planetary nebulae.

However, the frequency of super novae exceeds (if the recurrent picture is the correct one) or is at least comparable with (if a merger follows the outburst) the Galactic Type I and Type II supernova frequencies that have been inferred from the observations and one wonders why super novae have not been clearly identified observationally. It may be that their relative dimness at optical wavelengths has prevented discovery (and/or identification).

The distinctly different final outcomes of the recurrent scenario (a helium-rich planetary nebula) and of the merger scenario (an R CrB star surrounded by an expanding helium shell) provide an opportunity for the observational astronomer to settle a question which, from the theoretical point of view, is quite open.

Perhaps the safest prediction as to the terminal evolution of helium-star cataclysmics (after flashes have ceased) comes from an examination of the properties of the binary system GP Com, with an orbital period of 46.5 minutes and an estimated mass transfer rate of $\sim 2 \times 10^{-11}\ M_\odot$ yr^{-1} (Nather, Robinson, & Stover 1981), and of the properties of the system HZ-29 (AM CVn), with a period 17.5 minutes and estimated mass transfer rate of $\sim 5 \times 10^{-10}\ M_\odot$ yr^{-1} (Faulkner et al. 1972). These systems are most easily understood in terms of the transfer of essentially pure helium from a very low mass (~ 0.001–$0.01\ M_\odot$) helium degenerate dwarf to a much more massive CO degenerate dwarf companion. The amount of mass remaining to be transferred and the rate of transfer are so small that one does not expect the excitation of another helium shell flash. Thus, one may surmise from a combination of observational and theoretical evidence that recurrent helium-star cataclysmics evolve into single white dwarfs of mass of the order of 0.6–$0.8\ M_\odot$.

The two known HeCVs are placed in Figure 15 along with

the low-mass X-ray binary 1820−30. In this same figure are four evolutionary tracks for close binaries consisting initially of a degenerate dwarf accreting various fuels from a companion (the solid track has been discussed in the previous section). Each track is labeled according to the format: initial donor mass (composition of donor) + initial accretor mass. Model tracks for the two cases in which the donor is a hydrogen star are from Tutukov et al. (1987); in one instance the donor is unevolved (*dashed track*) and in the other it is slightly evolved when mass transfer begins (*dotted track*). The other two tracks are from Tutukov & Fedorova (1989); in one case, the donor is a nondegenerate helium star, and in the other, the donor is a degenerate CO dwarf. All four theoretical tracks converge onto the line describing the evolution of a low-mass binary with a degenerate donor of mass less than $\sim 0.1\ M_\odot$. Even allowing for possibly large errors in the estimates of accretion rates, all three observed systems lie close to the convergent solution for very low mass degenerate donors, and this circumstance makes it impossible to draw a firm conclusion as to the prior history of these systems based only on placement in this diagram. However, in the cases of AM CVn and GP Com, the presence of helium in their spectra excludes the scenario involving a CO donor. The two surviving scenarios (initial nondegenerate hydrogen star or helium star) both predict the transfer of pure helium and therefore the occurrence of helium shell flashes during previous evolution. The fact that the systems have remained binaries following shell flashes demonstrates that the common envelope formed in consequence of a flash does not lead to dissolution of the donor. Components of mass small than $\sim 0.01\ M_\odot$, as observed for AM CVn and GP Com, develop a deep convective envelope (Tutukov & Fedorova 1989) which makes them unstable to dynamical disintegration by the Ruderman-Shaham (1985) mechanism.

7. SUMMARY AND CONCLUSION

Modern scenarios for close binary star evolution suggest that up to 10% of nondegenerate helium stars known observationally as sdB–sdO stars are members of close binaries with component separations less than 10 solar radii and orbital periods less than several days. It is quite possible that the other 90% are the descendants of binaries consisting of two very close helium dwarfs which have merged under the influence of gravitational wave radiation. A fraction of all helium stars in binaries have companions which are degenerate CO or ONe dwarfs and some of these systems are so close that, due to angular momentum losses by the radiation of gravitational waves, the helium component can fill its Roche lobe during the core helium-burning phase. The frequency of formation of such semidetached binaries in our Galaxy is about $0.01\ \mathrm{yr}^{-1}$.

These systems experience two distinct phases of mass transfer (Tutukov & Fedorova 1989). During the first phase, mass transfer takes place at a nearly constant rate of $3 \times 10^{-8}\ \mathrm{yr}^{-1}$ (Iben & Tutukov 1987). The orbital period decreases with time (to a minimum of ~ 13 minutes) and interruptions occur in consequence of helium shell flashes when the accreted layer exceeds a critical mass. The total duration of this phase is $\sim 10^7$ yr. Regretfully, we do not know as yet of any real systems in the quiescent phase of the first stage of mass exchange. On the other hand, the historical records contain one possible example of an interruption which occurs when the accreted layer exceeds a critical mass above a degenerate dwarf more massive than $0.8\ M_\odot$. This example is the star S Andromeda (SN 1885A), the only supernova thus far observed in Andromeda. Chugai (1983) and Chevalier & Plait (1988) have remarked on the unusually low brightness and short lifetime of this supernova. Chevalier & Plait (1988) conclude that the total energy of S And is only $\sim 4 \times 10^{50}$ ergs, which corresponds to the energy liberated by burning $\sim 0.1\ M_\odot$ of helium. We note that half of the critical accreted mass of $\sim 0.13\ M_\odot$ which we estimate for a CO dwarf accretor more massive than $\sim 0.8\ M_\odot$ is consistent with $\sim 0.1\ M_\odot$. Recently it has been shown that the remnant of this supernova is an obscuring cloud which emits radiation in Fe I lines (Fesen, Hamilton, & Sack 1989). Multiplying the current expansion velocity of 5000 km s^{-1} by 100 yr, we have that the neutral iron remnant is approximately one parsec in diameter. If this remnant has optical depth unity, the amount of Fe I in it is about $0.04\ M_\odot$. Some of the iron in the remnant is in the form of grains and ionized iron is found outside of the region containing Fe I. The mass of the iron grains must be less than $0.1\ M_\odot$ as these grains do not contribute appreciably to the obscuration. Thus, the properties the remnant provide further support for the identification of S And as the outburst of a massive helium star cataclysmic system, with the formation of an ejected shell of iron which is substantially smaller than that produced by, say, a Type Ia supernova.

During the second, or slower accretion phase, which lasts for several times 10^8 yr, the orbital period increases (up to ~ 40 minutes) and the mass exchange rate drops to as low as $\sim 10^{-11}\ \mathrm{yr}^{-1}$ (Tutukov & Fedorova 1989). It is possible that observational analogs of systems in the second stage are the cataclysmics AM CVn (HZ-29) with $P_{\mathrm{orb}} = 17.5$ minutes and GP Com with $P_{\mathrm{orb}} = 46.5$ minutes. These systems show no lines of hydrogen in their spectra. Another example of a system in the slow accretion phase, but with a neutron star as accretor, may be the star PS 1820−30, with an orbital period of 11 minutes (Priedhorsky et al. 1986), but the identification is not unique since a similar system can be achieved by invoking a donor that is an evolved hydrogen star (Tutukov et al. 1987).

The thermal evolution of the helium shell accumulated at the rate $3 \times 10^{-8}\ M_\odot\ \mathrm{yr}^{-1}$ by a cold CO degenerate dwarf differs substantially from the thermal evolution of the hydrogen shell accumulated by a cold white dwarf in classical cataclysmic systems. In the helium-accretion situation, the high thermal conductivity in both the accreted layer and in the underlying degenerate dwarf has the consequence that much more energy flows inward as well as outward from the accreted layer than remains within the layer and this keeps the temperature in the accreted layer from rising as rapidly with increasing accumulated mass as one might have expected from experience with classical cataclysmics. In particular, the critical mass of accumulated matter for producing a thermonuclear runaway depends very weakly on the initial mass of the cold accretor, in strong contrast with the case of classical cataclysmics. The critical shell mass necessary for exciting the first helium thermonuclear runaway changes only by $0.02\ M_\odot$, from $0.15\ M_\odot$ to $0.13\ M_\odot$, as initial accretor mass is increased from $0.6\ M_\odot$ to $1.0\ M_\odot$. Because we have neglected effects such as shear mixing between matter at the edge of the accretor and accreted matter (which may dredge carbon up into the accreted layer) and the rotation of the accretor, these numbers are, of course, only first approximations to what will occur in real situations, but the development of a critical shell of substantial mass in the case of an initially very cold accretor seems inevitable.

The various possible evolutionary paths for helium-star

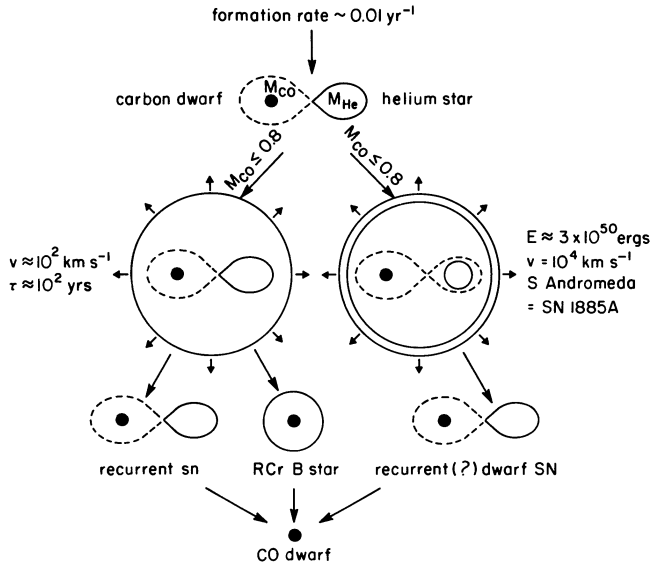

FIG. 16.—Scenario schematic for the evolution of helium cataclysmics

cataclysmics are summarized in Figure 16. The result of the first helium thermonuclear runaway depends entirely on the initial mass of the accreting degenerate dwarf. The explosion initiated in the shell of helium accreted on a massive degenerate dwarf ($M_{CO} > 0.8\ M_\odot$, occurrence frequency $\nu \sim 0.002$ yr^{-1}) has the character of a (dwarf) supernova, but helium ignition in the shell accreted by a low mass degenerate dwarf ($M_{CO} < 0.8\ M_\odot$, $\nu \sim 0.008$ yr^{-1}) leads to the quasi-static expansion of the helium envelope beyond the dimensions of the orbit, with the consequent loss of that envelope due to friction between matter in the envelope and the interior stellar cores—the donor and the core of the accretor. If the helium donor is dissolved in the common envelope, the system will evolve into a single star resembling an R CrB star. On the other hand, the existence of helium donors in the highly evolved systems GP Com and AM CVn can be argued as evidence for the survival of the helium donor during a prior helium shell flash (or flashes). In spite of this argument, we retain in Figure 16 the option of forming an R CrB star.

Several problems remain to be solved. Yet to be determined is the precise value of the critical CO degenerate dwarf mass M_{crit} that defines the border between systems which experience a (dwarf) supernova outburst and systems which experience a super nova outburst. Our estimate of 0.8 $M_\odot$ is based on a calculation by Khokhlov (1990). Although it is clear that a deflagration or detonation wave will incinerate and expel the outer half of the accreted shell in those systems with $M_{CO} > M_{crit}$, it is not clear whether a detonation or deflagration wave will propagate inward, incinerating the entire accretor (Nomoto 1982b). Thus, we do not know theoretically whether such systems evolve into full-fledged supernovae or instead evolve into dwarf supernovae. The properties of SN 1885A in Andromeda might be taken to suggest that the latter possibility is the more likely one, except that we have not demonstrated conclusively that the precursor of S And was a helium-star cataclysmic.

The chemical composition of the matter lost in both cases is of special interest. The total amount of matter processed by helium star cataclysmics every year is of the order of $dM/dt \sim 0.5\ M_\odot \times 0.01$ yr^{-1} = $0.005\ M_\odot$ yr^{-1}. This is to be compared with the rate at which normal cataclysmics process matter ($\sim 0.003\ M_\odot$ yr^{-1}), the rate at which normal supernovae process matter ($\sim 0.02\ M_\odot$ yr^{-1}), and the rate at which old stars process matter ($\sim 0.5\ M_\odot$ yr^{-1}). These estimates show that the ejecta of helium star cataclysmics cannot significantly contribute to the formation of the abundant elements produced by "normal" stars, but they could contribute ($\sim$20%) to the store of *s*-process isotopes in the Galaxy. However, the distribution of these isotopes will not be in the solar system distribution, as is the case with the distribution produced by AGB stars, and this establishes an upper limit on any estimated rate at which helium-star cataclysmics process matter. Our estimate of a 20% contribution is large enough that nucleosynthesis calculations should be carried out to determine the detailed characteristics of the distribution of neutron-rich isotopes formed by the super novae which result from helium star cataclysmics in which the degenerate dwarf accretor has an initial mass in excess of $\sim 0.8\ M_\odot$.

REFERENCES

Barone, F., Milano, L., Russo, G., & Sarna, M. J. 1988, preprint
Chevalier, R. A., & Plait, P. C. 1988, ApJ, 331, L109
Chugai, N. N. 1983, Astron. Tsirk., No. 1263, 3
Despain, K. H. 1981, ApJ, 251, 639
Ergma, E., Rahunen, T., & Vilhu, O. 1978, Nauchneye Inform., 45, 159
Ergma, E., & Tutukov, A. V. 1980, A&A, 84, 123
Faulkner, J. 1971, ApJ, 170, L99
Faulkner, J., Flannery, B. P., & Warner, B. 1972, ApJ, 175, L79
Fesen, R. A., Hamilton, A. J. S., & Saken, J. M. 1989, ApJ, 341, 155
Fujimoto, M. Y. 1980, in Type I Supernovae, ed. J. C. Wheeler (Austin: University of Texas), 115
Fujimoto, M. Y., Hanawa, T., Iben, I., Jr., & Richardson, M. B. 1984, ApJ, 278, 813
Fujimoto, M. Y., Iben, I., Jr., & Hollowell, D. 1990, ApJ, 349, 580
Fujimoto, M. Y., & Sugimoto, D. 1982, ApJ, 257, 291
Gallino, R., Busso, M., Picchio, G., Raiteri, C. M., & Renzini, A. 1988, ApJ, 344, L45.
Hashimoto, M., Nomoto, K., Arai, K., & Kaminisi, K. 1986, ApJ, 307, 687
Hollowell, D., & Iben, I., Jr. 1988, ApJ, 333, L25
———. 1989, ApJ, 340, 966
Iben, I., Jr. 1975, ApJ, 196, 525
———. 1981, ApJ, 243, 987
———. 1990, ApJ, 353, 215
Iben, I., Jr., Nomoto, K., Tornambè, A., & Tutukov, A. V. 1987, ApJ, 317, 717
Iben, I., Jr., & Tutukov, A. V. 1984a, ApJS, 54, 335
———. 1984b, in High Energy Transients, ed. S. Woosley (NY: AIP), 232
Iben, I., Jr., & Tutukov, A. V. 1984c, ApJ, 284, 719
———. 1985, ApJS, 58, 661
———. 1987, ApJ, 313, 727
———. 1989a, in IAU Colloquium 131, Planetary Nebulae, ed. S. Torres-Peimbert (Dordrecht: Kluwer), 505
———. 1989b, ApJ, 342, 430
———. 1990, in Frontiers of Stellar Astronomy, ed. D. L. Lambert (Austin: University of Texas)
Käppeler, K., Gallino, R., Busso, M., Picchio, G., & Raiteri, C. M. 1990, ApJ, 354, 630
Khokhlov, A. M. 1990, Astr. Zh., in press
Lambert, D. L. 1989, in Evolution of Peculiar Red Giants, ed. H. R. Johnson & B. Zuckerman (Cambridge: Cambridge Univ.), 101
Livio, M., & Soker, N. 1988, ApJ, 329, 764
Maeder, A., & Meynet, G. 1989, A&A, 210, 155
Mengel, J. G., & Sweigart, A. V. 1981, in Astrophysical Parameters for Globular Clusters, ed. A. G. D. Philip (Dordrecht: Reidel), 277
Meyer, F. 1986, in IAU Colloquium 89, Radiation Hydrodynamics in Stars and Compact Objects, ed. D. Mihalas (Lecture Notes Phys., 255), 249
Meyer, F., & Meyer-Hofmeister, E. 1979, A&A, 78, 176
Nather, R. E., Robinson, E. L., & Stover, R. J. 1981, ApJ, 244, 269
Nomoto, K. 1980, in Type I Supernovae, ed. J. C. Wheeler (Austin: University of Texas), 164
———. 1982a, ApJ, 253, 798
———. 1982b, ApJ, 257, 780
Nomoto, K. 1984, ApJ, 277, 791

Paczyński, B. 1967, Acta Astr., 17, 287
———. 1976, in IAU Symposium 73, The Structure and Evolution of Close Binary Systems, ed. P. Eggleton, S. Mitton, & J. Whelan (Dordrecht: Reidel), 75
Priedhorsky, W., Sella, L., & White, N. E. 1986, ApJ, 312, L17
Ruderman, M. A., & Shaham, J. 1985, ApJ, 289, 244
Saffer, R. A., & Liebert, J. 1989, in White Dwarfs, ed. G. Wegner (Lecture Notes Phys., 328), 408
Savonije, G. J., de Kool, M., & van den Heuvel, E. P. J. 1986, A&A, 155, 51
Smak, J. 1983, ActA, 33, 333
Smith, V., & Lambert, D. 1986, ApJ, 311, 843
Taam, R. E. 1980a, ApJ, 237, 142
———. 1980b, ApJ, 242, 749
Taam, R. E., & Bodenheimer, P. 1989, ApJ, 337, 849
Tornambè, A., & Matteucci, F. 1986, MNRAS, 223, 69
Tutukov, A. V. 1988, Astrophysics, 28, 359
Tutukov, A. V., & Fedorova, A. V. 1989, Astr. Zh., 66, 1172
Tutukov, A. V., Fedorova, A. V., Ergma, E. V., & Yungelson, L. R. 1987, Soviet Astr. Letters, 13, 328
Tutukov, A. V., & Yungelson, L. R. 1972, Soviet AJ, 8, 227
———. 1979, Acta Astr., 29, 666
———. 1987a, Comments Ap., 12, 57
———. 1987b, in The Second Conference on Faint Blue Stars, ed. A. G. Davis Philip, D. S. Hayes, & J. Liebert (Schenectady: L. Davis), 435
———. 1988a, Nauch. Inf., 65, 30
———. 1988b, Soviet Astr. Letters, 14, 265
———. 1990, Sov. Astr. Letters, 67, 109
van den Bergh, S., McClure, R. D., & Evans, R. 1987, ApJ, 323, 44
Webbink, R. 1984, ApJ, 277, 355